Constraint modified time dependent failure assessment diagram (TDFAD) based on $C(t)$-$A_2(t)$ theory for creep crack

Yanwei Dai[1]

Institute of Electronics Packaging Technology and Reliability,
College of Mechanical Engineering and Applied Electronics Technology,
Beijing University of Technology, Beijing 100124, China
ywdai@bjut.edu.cn

Yinghua Liu

Department of Engineering Mechanics, AML, Tsinghua University, Beijing 100084, China

Fei Qin

Institute of Electronics Packaging Technology and Reliability,
College of Mechanical Engineering and Applied Electronics Technology,
Beijing University of Technology, Beijing 100124, China

Yuh J. Chao

Department of Mechanical Engineering, University of South Carolina, 300 S. Main Street Columbia, SC 29208, USA

Haofeng Chen

Department of Mechanical & Aerospace Engineering, University of Strathclyde, Glasgow, G1 1XJ, UK

[1] Corresponding author: ywdai@bjut.edu.cn;

Abstract

Due to the potential influence of constraint effect on failure assessment, a link is needed to bridge the constraint effect characterized by higher order term asymptotic solution and time dependent failure assessment diagram (TDFAD). In this paper, a modification method for creep toughness incorporating $C(t)$-$A_2(t)$ theory is proposed based on Nikbin-Smith-Webster model. The relation between Q-term and $A_2(t)$-term is also presented for creep crack. Results show that the creep toughness can be influenced by constraint parameter remarkably. A modified TDFAD is proposed based on $C(t)$-$A_2(t)$ solution. Based on the creep data of 316H stainless steel and various compact tension specimens, the modified TDFAD curves considering constraint effect characterized with $A_2(t)$-term is presented and discussed, which indicates the important role of constraint effect on the assessment boundary of TDFAD. The research given in this paper can provide an alternative method in which the constraint effect can be included in TDFAD under high temperature.

Keywords: TDFAD; Creep toughness; Constraint effect; A_2^*-parameter; CT specimen.

1 Introduction

Accurate lifetime assessment of serviced components at elevated temperature is an important topic which has been concerned by some engineers and scientists [1, 2]. There are some fitting-for-service codes which have been developed for engineering evaluations for crack contained structures under various conditions, e.g. R6 [3], R5 [4], SINTAP [5, 6], FITNET [7] and so forth. Due to the influence of creep damage as well as the increase of demands on gaseous emission reduction and energy saving, lifetime prediction and failure assessment for structural components at elevated temperature have recently drawn a lot of attentions.

Failure assessment diagram (FAD) [8, 9] is a kind of assessment method which is related with the fracture toughness and fracture parameters, e.g. stress intensity factor (SIF) K and J-integral. Under creep condition, the fracture parameter is the J-analogy parameter which is defined as $C(t)$-integral (or C^*-integral under extensive creep) [10]. FAD was extended to creep regime by Ainsworth and coworkers [11, 12] with definition of time dependent failure assessment diagram (TDFAD) in which creep mechanism is incorporated. TDFAD has been extended to some fields of engineering assessment, e.g. evaluation of weldments through TDFAD was given by Xuan et al. [13] based on the equivalent homogeneous model. Prediction of crack initiation for 316H stainless steel via TDFAD technique was given by Davies et al. [14], and similar method can be found for austenitic and ferritic steels [15]. The discussions on development of R5 and TDFAD at high temperature were given by Dean et al. [16].

For crack contained structure at high temperature, the stress field of crack tip could be influenced by the specimen size, crack depth and even material mismatch which are attributed as the “constraint effect” [17-21]. It should be pointed out that the “constraint effect” can lead to the variations of fracture toughness, which can finally affect the assessment boundaries for curves of FAD and TDFAD. It indicates the significant influence of constraint effect on TDFAD curves, which may eventually lead to the change of assessment solutions (over conservative or non-conservative). Although

studies on the influence of constraint effect on FAD curves have been investigated widely [22-24], however, the investigations on the influence of constraint effect on the assessment boundary of TDFAD under high temperature are not that fruitful in the available literatures.

Based on constraint parameter Q [2, 25], Budden and Ainsworth [26] made a modification on TDFAD with consideration of constraint effect for creep crack, where the modification was based on the definition of creep toughness $K_{\mathrm{mat}}^{\mathrm{c}}$ [12] at high temperature instead of fracture toughness K_{IC}. Some investigations on the creep toughness for different materials can be found in [12, 15, 27-29]. Except for Q-parameter, some constraint theories have also been presented for creep crack under various conditions, e.g. $A_2(t)$-parameter [17, 19, 30, 31] based on strictly higher order asymptotic solutions which are solved with nonlinear analysis and solving [32-34]. Dai et al. [35] presented a modified TDFAD for mode II creep crack based on stress damage model. There are also some other constraint theories, e.g. parameter considering blunting mechanism [36], unified parameter [37], load independent parameter [38] and parameter considering out-of-plane effect [39]. Though different constraint parameters have been proposed, the discussions on the influence of constraint effect on TDFAD curves based on those higher order asymptotic solutions as well as the investigations on embedding those constraint theories to TDFAD curves are very limited.

The objective of this paper is to present a modification method on TDFAD curves incorporating with constraint effect based on $A_2(t)$-parameter. Towards this aim, the overall content of this paper is organized as follows. The TDFAD method is revisited in Section 2 in which the basic concepts of TDFAD curves and creep toughness are illustrated. In Section 3, the relation between constraint parameter $A_2(t)$ and Q is derived and discussed. The modification on creep toughness based on $A_2(t)$-parameter is presented in Section 4. The modified TDFAD based on $A_2(t)$-parameter for creep crack is proposed in Section 5. Numerical cases with different compact tension

(CT) specimens are given in Section 6. With characterizations of constraint effect for various CT specimens, modified TDFAD curves are also presented in Section 6 where the effect of $A_2(t)$-parameter on assessment boundary for TDFAD curve is also discussed in this section. The conclusions are drawn in the last section.

2 Revisit of time dependent failure assessment diagram (TDFAD)

If the primary load is considered only, the two coordinates of the FAD, i.e. K_r and L_r, can be presented as [3]

$$K_r = \frac{K}{K_{\mathrm{IC}}} \tag{1}$$

$$L_r = \frac{P}{P_L} \tag{2}$$

where K and K_{IC} in Eq. (1) are the stress intensity factor (SIF) and fracture toughness, respectively. P and P_L in Eq. (2) are the applied load and limit load of the analysed component.

For FAD, there are three option curves to be selected for FAD in R6, i.e. option 1 curve, option 2 curve and option 3 curve. The option 1 curve is a function that is independent of material properties and presented as [11]

$$F_1(L_r) = \left(1-0.14L_r^2\right)\left[0.3+0.7\exp\left(-0.65L_r^6\right)\right] \tag{3}$$

Considering long time creep, Ainsworth [12] presented another alternative formula to substitute Eq.(3), and the formula can be given as

$$F_1(L_r) = \left(1-0.2L_r^2\right)\left[0.35+0.65\exp\left(-1.4L_r^6\right)\right] \tag{4}$$

Eq. (4) is a fixed curve which is independent on constraint effect.

With consideration of R6 option 2, K_r can be described by L_r as [3]

$$K_r = F_2(L_r) = \left[\frac{E\varepsilon_{\mathrm{ref}}}{\sigma_{\mathrm{ref}}} + \frac{L_r^2\sigma_{\mathrm{ref}}}{2E\varepsilon_{\mathrm{ref}}}\right]^{-1/2} \tag{5}$$

where E is the Young's modulus, ε_{ref} is the reference strain and σ_{ref} is the reference stress (see Fig. 1). The reference stress can be determined by $\sigma_{\text{ref}} = L_r \cdot \sigma_y$, and σ_y here is the yield stress. The option 3 of R6 can be given as

$$K_r \le F_3\left(L_r\right) = \left(J_e / J\right)^{1/2} \tag{6}$$

where J_e is the *J*-integral under linear elastic condition and *J* is the *J*-integral under elastoplastic range. In fact, the option curves 1-3 are representatives of three different failure modes, i.e. the linear elastic fracture mode, elastoplastic fracture and plastic collapse.

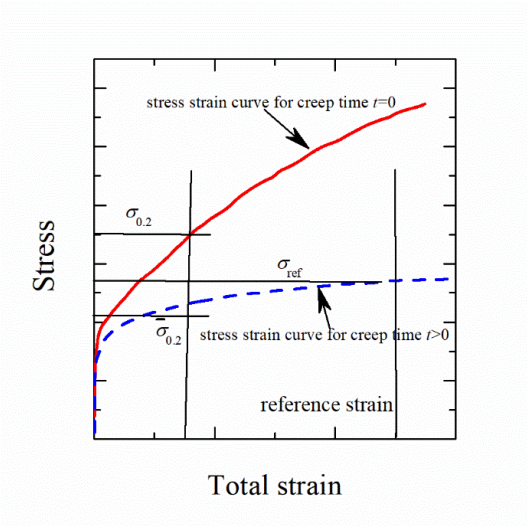

Fig. 1 Definitions of different kinds of stresses adopted in TDFAD curves

The option 1 curve can't be influenced by material properties and specimen geometry. As for option 3 curve, it can be affected by specimen geometry and loading level. The option 2 curve is dependent on its material properties and its loading levels, i.e. it could be influenced by constraint effect. Hence, option 2 curve is investigated emphatically in this paper.

TDFAD is extended from FAD in which creep time and the creep damage caused by high temperature is taken into consideration for TDFAD curves. For TDFAD, Eq. (1) will be represented as below by replacing K_{IC} with creep toughness $K^{\text{c}}_{\text{mat}}$.

$$K_r = \frac{K}{K^{\text{c}}_{\text{mat}}} \tag{7}$$

where $K_{\mathrm{mat}}^{\mathrm{c}}$ can be presented as [12]

$$K_{\mathrm{mat}}^{\mathrm{c}}=\left[K^{2}+\frac{n}{n+1}\frac{EP\Delta_{\mathrm{c}}}{B_{n}\left(W-a\right)}\eta\right]^{1/2} \tag{8}$$

in which Δ_{c} is the load line displacement with a creep crack growth of Δa, B_n is the specimen net thickness, W is the width of the specimen and η is a function given in ASTM 1457-13 [40]. With Eq. (2), the L_r at elevated temperature can be obtained as

$$L_{r}=\frac{\sigma_{\mathrm{ref}}}{\bar{\sigma}_{0.2}} \tag{9}$$

where $\bar{\sigma}_{0.2}$ is the so called 0.2% creep strength (see Fig. 1) which is determined by isochronous stress strain curve at a fixed temperature. With Eqs. (5)-(9), the TDFAD curve at a fixed creep time, e.g. creep time $t>0$, can be given as following:

$$K_{r}=\left[\frac{E\varepsilon_{\mathrm{ref}}}{L_{r}\bar{\sigma}_{0.2}}+\frac{L_{r}^{3}\bar{\sigma}_{0.2}}{2E\varepsilon_{\mathrm{ref}}}\right]^{-1/2}\qquad \text{for } L_{r}\le L_{r}^{\max} \tag{10}$$

$$K_{r}=0\quad \text{for } L_{r}>L_{r}^{\max} \tag{11}$$

where $L_r^{\max}$ is therefore given by

$$L_{r}^{\max}=\frac{\sigma_{f}}{\bar{\sigma}_{0.2}} \tag{12}$$

σ_f here is the creep rupture stress. In TDFAD curve, the fracture modes can be attributed as creep fracture and plastic collapse, respectively. Eqs. (10)-(12) can be determined by its mechanical properties for a specific material.

3 Novel insights into constraint effect characterization for creep crack

The well known constitutive equation with power-law form can be presented as [41]

$$\dot{\varepsilon} = \frac{\dot{\sigma}}{E} + \dot{\varepsilon}_0 \left(\frac{\sigma}{\sigma_0} \right)^n \tag{13}$$

where $\dot{\varepsilon}$ is the strain rate, $\dot{\sigma}$ is the stress rate, $\dot{\varepsilon}_0$ is the reference strain rate, σ_0 is the reference stress and n is the creep exponent. In general, the creep strain is much greater than the elastic strain under extensive creep, and Eq.(13) can be simplified as

$$\dot{\varepsilon}^c = A\sigma^n \tag{14}$$

in which A is the creep coefficient that equals to $\dot{\varepsilon}_0 / \sigma_0^n$.

For crack in power-law creeping solids, the stress field considering higher order term Q can be presented as below [2, 26]

$$\sigma_{ij} = \sigma_0 \left(\frac{C(t)}{\sigma_0 \dot{\varepsilon}_0 I_n r} \right)^{1/(n+1)} \tilde{\sigma}_{ij}(n,\theta) + Q\sigma_0 \delta_{ij} \tag{15}$$

where $C(t)$ is the $C(t)$-integral, I_n is the integral constant related with crack front stress state, r is the distance from crack tip, $\tilde{\sigma}_{ij}(n,\theta)$ is the angular dimensionless function and Q is the constraint parameter defined in [2, 26].

The three order termed expansion for mode I creep crack was given by Chao et al. [30] which can be presented as

$$\sigma_{ij}(r,\theta) = A_1(t)\Lambda^{s_1}\tilde{\sigma}_{ij}^{(1)}(\theta) + A_1(t)\left[A_2(t)\Lambda^{s_2}\tilde{\sigma}_{ij}^{(2)}(\theta) + \left(A_2(t)\right)^2 \Lambda^{s_3}\tilde{\sigma}_{ij}^{(3)}(\theta) \right] \tag{16}$$

where $\Lambda = r/L$, L is the characteristic length, s_i and $\tilde{\sigma}_{ij}^{(i)}(\theta)$ (i=1, 2, 3) here are the singular exponent and angular dimensionless function. Note that $A_1(t)$ -term and $A_2(t)$-term are respectively denoted as A_1^* and A_2^* if crack front is under extensive creep. Herein, A_2^* is the higher order term or the so-called constraint parameter which can be determined by point match method [30, 42]. A_1^* is defined as

$$A_1^* = \left(\frac{C^*}{AI_n L} \right)^{1/(n+1)} \tag{17}$$

Thus, the first term of Eq. (16) can be derived as

$$A_1^* \Lambda^{s_1} \tilde{\sigma}_{ij}^{(1)}(\theta) = \sigma_0 \left(\frac{C^*}{\sigma_0 \dot{\varepsilon}_0 I_n r} \right)^{1/(n+1)} \left(\frac{1}{L} \right)^{-2/(n+1)} \tilde{\sigma}_{ij}^{(1)}(\theta) \tag{18}$$

Comparing Eq. (16) with Eq. (15), the following relationship can be obtained if the first terms of them are assumed to be HRR type and L=1 mm in Eq. (18), i.e.

$$Q\sigma_0 \delta_{ij} = A_1^* \left[A_2^* r^{s_2} \tilde{\sigma}_{ij}^{(2)}(\theta) + \left(A_2^* \right)^2 r^{s_3} \tilde{\sigma}_{ij}^{(3)}(\theta) \right] \tag{19}$$

The relationship between second order term constraint parameter Q and third order termed constraint parameter A_2^* can be established through Eq. (19). The relation between Q and A_2 under elastoplastic conditions has been presented by Ding and Wang [43]. The advantage to use A_2^*-parameter instead of Q-parameter is obvious, e.g. A_2^* can be determined directly through numerical analysis for a specific cracked geometry.

4 Creep toughness modification based on ductility model with A_2^* -parameter

Due to the role of creep toughness in TDFAD curves, a creep crack growth (CCG) rate is needed to introduce so as to obtain the creep toughness. Herein, the Nikbin-Smith-Webster (NSW) [44] model is given as below, which is adopted to predict the creep crack growth rate, i.e.

$$\dot{a}_{\mathrm{NSW}} = \frac{n+1}{\varepsilon_f^*} \left[\frac{C^*}{I_n} \right]^{n/(n+1)} \left(A r_{\mathrm{c}} \right)^{1/(n+1)} \tag{20}$$

where r_{c} is the creep process zone size and ε_f^* is the multiaxial ductility. The computation of ε_f^* can be obtained through definition of multiaxial strain factor (MSF) [45] which can be presented as:

$$\frac{\varepsilon_f^*}{\varepsilon_f} = \sinh\left[\frac{2}{3} \left(\frac{n-1/2}{n+1/2} \right) \right] \Big/ \sinh\left[2h \left(\frac{n-1/2}{n+1/2} \right) \right] \tag{21}$$

in which voids growth mechanism can be considered in Eq. (21). Herein, ε_f and h are the failure strain and stress triaxiality, respectively. h is defined as the ratio between

hydrostatic stress and equivalent stress, i.e. $h=\sigma_m/\sigma_e$.

If the constraint effect of creep crack is taken into account, the creep crack growth (CCG) rate with modification of *Q*-parameter based on NSW model is given as [26, 46, 47]

$$\dot{a}=\dot{a}_{\mathrm{NSW}}\cdot g \tag{22}$$

where factor g is defined as

$$g=1-\frac{d\varepsilon_f^*}{dh}\frac{1}{\varepsilon_f^*(\theta,n)}\frac{Q}{2\tilde{\sigma}_e(\theta,n)}\left(\frac{C^*}{\sigma_0\dot{\varepsilon}_0 I_n}\right)^{-1/(n+1)} r_{\mathrm{c}}^{1/(n+1)} \tag{23}$$

It should be noted that the derivation of Eq. (23) is similar to the derivation given by Budden and Ainsworth [26], and the detail derivation has been listed in Appendix A. Based on the relations between *Q*-parameter and A_2^*-parameter derived in Section 3, the novel modification factor g' is proposed as:

$$g'=1-\frac{d\varepsilon_f^*}{dh}\frac{1}{\varepsilon_f^*(\theta,n)}\frac{\bar{\Lambda}}{2\tilde{\sigma}_e(\theta,n)}\left(\frac{C^*}{\sigma_0\dot{\varepsilon}_0 I_n}\right)^{-1/(n+1)} r_{\mathrm{c}}^{1/(n+1)} \tag{24}$$

in which $\bar{\Lambda}$ is identical to $\sigma_0^{-1}A_1^*\left[A_2^* r^{s_2}\tilde{\sigma}_{22}^{(2)}(\theta)+\left(A_2^*\right)^2 r^{s_3}\tilde{\sigma}_{22}^{(3)}(\theta)\right]$ and $\tilde{\sigma}_e(\theta,n)$ is the equivalent stress function. The differential of multiaxial ductility ε_f^* in Eq. (24) can be given as [44]

$$\frac{d\varepsilon_f^*}{dh}\frac{1}{\varepsilon_f^*(\theta,n)}=-2\left(\frac{n-0.5}{n+0.5}\right)\Big/\tanh\left[2h\left(\frac{n-0.5}{n+0.5}\right)\right] \tag{25}$$

With CCG rate estimation form given in Eq. (22), the creep crack growth length Δa for a creep crack can be presented as below by integrating creep time.

$$\Delta a=\dot{a}\cdot g'\cdot t \tag{26}$$

Herein, *t* is the creep time. With the dimensionless analysis of C^*-integral between creep crack growth assessment and reference stress method, the creep toughness with modification of $A_2(t)$ can be given as below:

$$K_{\mathrm{mat}}^{\bar{\Lambda}}=\left[E\left(\Delta a/bg'\right)^{1/q}t^{(1-1/q)}\right]^{1/2} \tag{27}$$

in which q is generally identical to $n/(n+1)$ according to Ref. [47]. The specific derivation of Eq. (27) can be found in Appendix B. b is the coefficient with CCG rate assessment of $\dot{a}=b(C^*)^q$ in general case. Therefore, the modified creep toughness $K_{\mathrm{mat}}^{\bar{\Lambda}}$ considering constraint effect and creep toughness $K_{\mathrm{mat}}^{\mathrm{c}}$ without considering constraint effect is presented as

$$K_{\mathrm{mat}}^{\bar{\Lambda}}=K_{\mathrm{mat}}^{\mathrm{c}}\cdot(g')^{-1/(2q)} \tag{28}$$

It should be noted that the determination of creep toughness $K_{\mathrm{mat}}^{\mathrm{c}}$ can be obtained experimentally, e.g. the experimental data of creep toughness for 316H stainless steel has been obtained by [15]. With the experimental data, the fitting curve of $K_{\mathrm{mat}}^{\mathrm{c}}$ for 316H steel can be seen in Fig. 2. In order to show the influence of constraint level on the creep toughness, the creep toughness of 316H stainless steel with four different levels of constraint levels are also presented in Fig. 2 in which shows that the variations of $K_{\mathrm{mat}}^{\bar{\Lambda}}$ with g', i.e. $g'=0.7$, 0.9, 1.1 and 1.3. It can be found that $K_{\mathrm{mat}}^{\bar{\Lambda}}$ increases with the decrease of modification factor. It means that the prediction curve of $K_{\mathrm{mat}}^{\bar{\Lambda}}$ will be underestimated for low constraint value specimen at different creep time if the constraint effect is not taken into account.

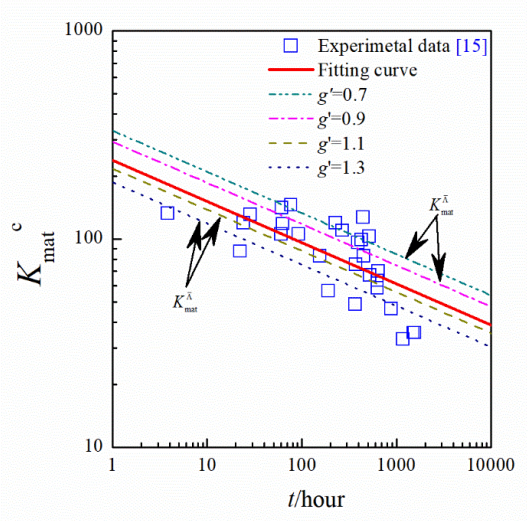

Fig. 2 Experimental data, fitting curve and prediction of $K_{\mathrm{mat}}^{\mathrm{c}}$ with different constraint modifications for 316H stainless steel

5 Modified TDFAD with higher order term solutions

With the modification of $K_{\text{mat}}^{\bar{\Lambda}}$ (see Eqs. (20)-(28)), a newly $\bar{K}_r$ is defined as below considering constraint effect so as to replace the previous K_r in the TDFAD, and $\bar{K}_r$ can be proposed as below:

$$\bar{K}_r = K_r \left(g'\right)^{1/(2q)} \tag{29}$$

Substituting (29) into Eq. (10), the TDFAD estimation curves incorporating with A_2^*-parameter are given as following.

$$\begin{cases} \bar{K}_r = \left[\dfrac{E\varepsilon_{\text{ref}}}{\bar{L}_r \bar{\sigma}_{0.2}} + \dfrac{\bar{L}_r^3 \bar{\sigma}_{0.2}}{2E\varepsilon_{\text{ref}}} \right]^{-1/2} \left(g'\right)^{1/(2q)} & \text{for } \bar{L}_r \le \bar{L}_r^{\max} \\ \bar{K}_r = 0 & \text{for } \bar{L}_r > \bar{L}_r^{\max} \end{cases} \tag{30}$$

where $\bar{L}_r$ is presented as

$$\bar{L}_r = L_r = \frac{P}{P_L} = \frac{\sigma_{\text{ref}}}{\bar{\sigma}_{0.2}} \tag{31}$$

The cut off line of the modified TDFAD curve is determined as $\bar{L}_r^{\max} = \sigma_f / \bar{\sigma}_{0.2}$. From Eq. (30), it can be found that the TDFAD curves will be influenced by the constraint effect which indicates that the estimation curves of TDFAD should change with the variations of constraint level for a cracked component.

To establish a TDFAD curve, some material properties are indispensably needed, e.g. rupture stress, proof stress, and ultimate strength and so on. Thus, the specific material properties in Eqs. (13), (14), (30) and (31) for 316H steel are listed in Table 1. The stress strain curves for 316H steel at 550 ℃ [15] is adopted here with various creep time (see Fig. 3). The isochronous stress-strain curve of 316H steel at different creep time are presented in Fig. 4.

Table 1 Material property used in calculation [15]

Material property	Value
Elastic modulus, *E*	140 GPa
Poisson's ratio, *v*	0.3

Flow stress, σ_0	306 MPa
0.2% proof stress, $\sigma_{0.2}$	170 MPa
Ultimate strength, σ_U	442 MPa
Failure strain, ε_f	37%
Creep exponent, *n*	11.58
Creep coefficient, *A*	1.47E-34 $MPa^{-n}h^{-1}$

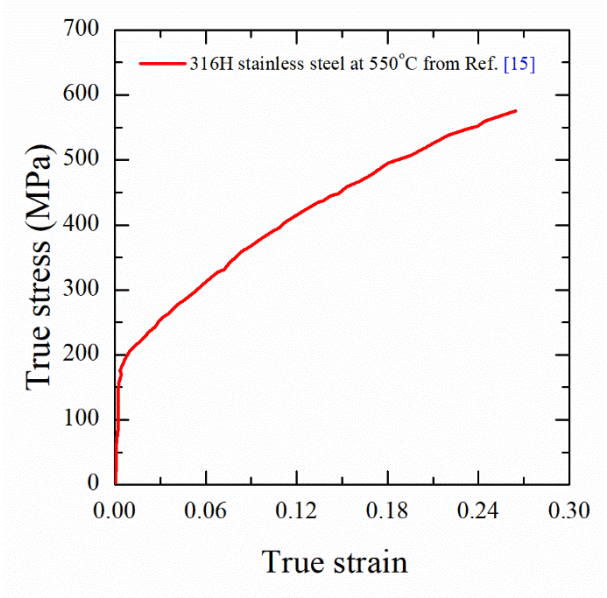

Fig. 3 True stress and true strain curve of 316H stainless steel at 550 ℃ [15]

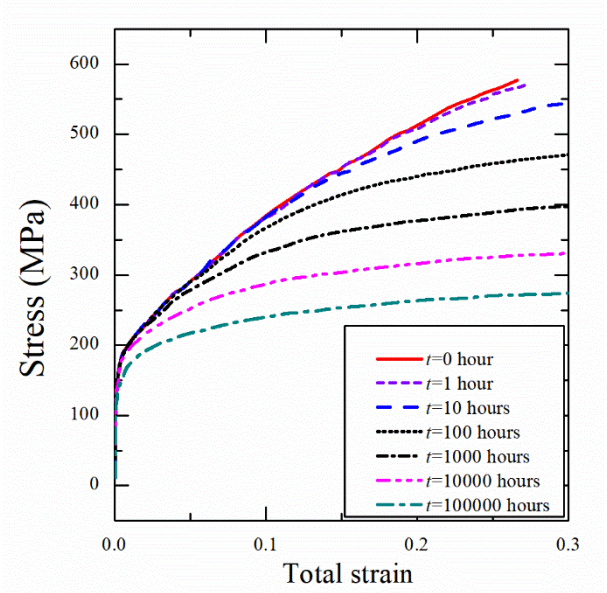

Fig. 4 Isochronous stress-strain curve of 316H stainless steel at different creep time [15]

The determination of rupture stress σ_f can be obtained by averaging proof stress

$\sigma_{0.2}$ and ultimate strength σ_U. The ultimate strength σ_U is obtained from the engineering stress strain curve of the material according to the definition of ultimate strength shown in Fig. 1. If the creep time is fixed, then the TDFAD curve can be determined. The TDFAD curves without constraint effect at various creep time *t* are shown in Fig. 5. Comparing the TDFAD curves at different creep time, e.g. 0 hour, 100 hours, and 1000 hours, it can be found that the borders of TDFAD curves do not change significantly which implies that 316H steel is a TDFAD insensitive material under various creep conditions. It also indicates that R6 curve could be an alternative method for short time creep assessment under high temperature for 316H steel. This phenomenon has also been validated by Davies [15]. It should be pointed out that the TDFAD curves in Fig. 5 do not take the constraint effect into account.

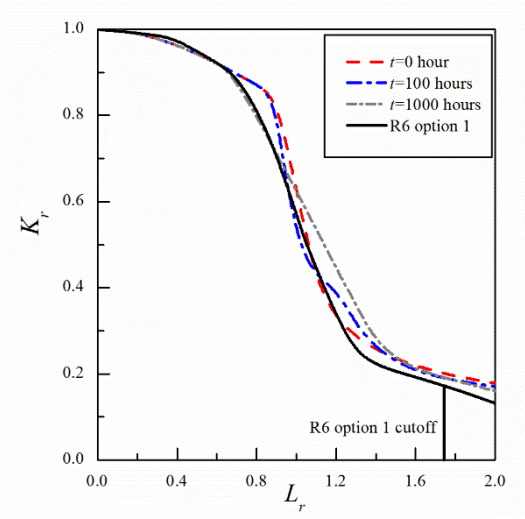

Fig. 5 Comparisons between R6 curve and TDFAD curves under different creep time

Comparisons of TDFAD curves including constraint effect with various conditions are given in Fig. 6. It can be found that the condition with $g'=1.1$ holds the broadest boundary comparing with the other conditions and the condition with $g'=0.9$ contains a rather smaller boundary. The estimation boundary under the condition with 10000 hours does not deviate from the R6 boundary significantly, which reflects the creep damage effect on the material properties at high temperature is not that remarkable for 316H stainless steel. Therefore, 316H stainless steel is a TDFAD insensitive material under creeping condition. The assessment boundaries with various

modification factor g' reflect the effect of constraint level on the TDFAD curves. The cut off line $L_r^{\max}$ here should not exceed the cutoff line defined in R6 [17], i.e. $L_r^{\max}=1.76$ for 316H steel under this condition. The reason is that the region for the cutoff line is based on mechanism of plastic collapse, and the cutoff line will be not influenced by constraint effect. The results given in Figs. 5-6 show that the level of constraint effect can affect the assessment border significantly even for the TDFAD insensitive material which implies the important role of constraint effect in fracture evaluation.

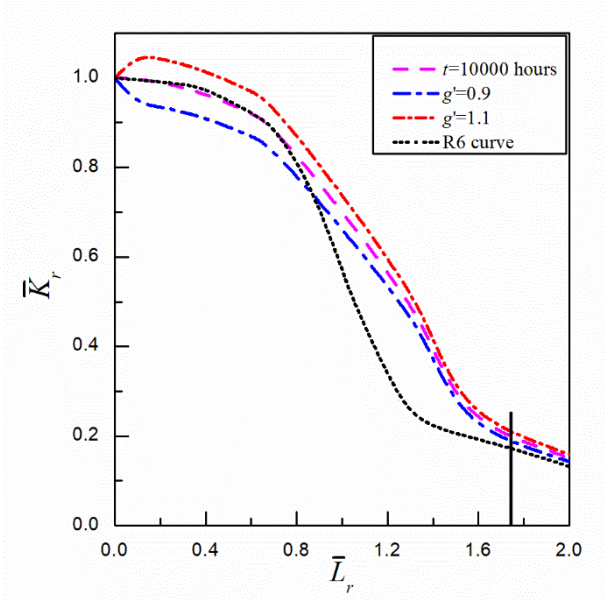

Fig. 6 Comparisons of TDFAD curves with R6 curve considering various conditions

6 Results and discussions

6.1 FE model, accuracy verification for SIFs and results of *C*(*t*)-integral

To present the influence of constraint effect on TDFAD curves, herein, compact tension (CT) specimen is selected as the computation case (shown in Fig. 7). The width (W) and height ($2H$) of the CT specimens are 40 mm and 48 mm, respectively. Two different cracked specimens with shallow and deep crack are adopted, i.e. shallow cracked CT specimen with a/W=0.15 and deep cracked CT specimen with a/W= 0.475

where those specimens are denoted as CT1, CT2, CT3 and CT4 so as to distinguish different loading conditions and crack depths. Detailed specimen sizes and loading levels can be seen in Table 2. The finite element (FE) code ABAQUS is adopted here to carry out the analysis. The element type is CPE4R and the FE meshes are shown in Fig. 7 (b). The total element numbers for CT1, CT2, CT3 and CT4 are 8377, 8377, 11808 and 11808, respectively. The loading conditions for those CT specimens are also given in Table 2.

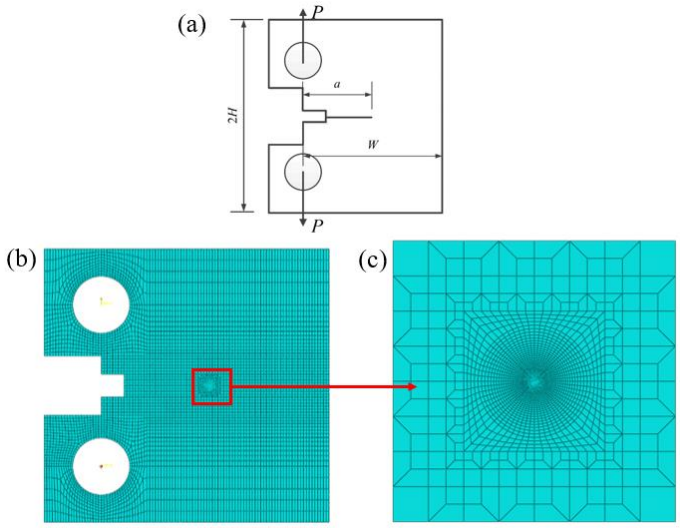

Fig. 7 Schematic diagram of (a) CT specimen geometry, (b) whole FE mesh and (c) crack tip mesh

Table 2 Fracture parameters used in calculation for CT specimens

Specimen	*a/W*	Load (N)	C^* (MPa · mm/h)	Time of *C*(t)-integral path independent (hours)
CT1	0.475	150	1.003E-05	1471.39
CT2	0.475	200	5.600E-05	511.88
CT3	0.15	300	5.460E-06	1900.46
CT4	0.15	350	2.911E-05	607.41

Table 3 Accuracy verification of the SIFs for the computed specimens

Specimen	ABAQUS	Tada et al. [48]	Relative Error
CT1	212.2	212.51	-0.94%
CT2	282.9	283.35	-0.99%
CT3	174.6	172.97	0.15%
CT4	203.8	201.80	0.16%

Table 2 presents geometry sizes and loadings of different CT specimens. Table 3 shows the accuracy of SIFs computed by ABAQUS in this paper compared with the

solutions for CT specimens given by Tada et al. [48] where their empirical expressions for CT specimens can be presented as

$$K_{\mathrm{I}} = Yf\left(a/W\right) \tag{32}$$

where Y and $f\left(a/W\right)$ can be represented as follows:

$$Y = \frac{P}{B_n W^{1/2}} \frac{2 + a/W}{\left(1 - a/W\right)^{3/2}} \tag{33}$$

$$f\left(a/W\right) = 0.886 + 4.64\left(a/W\right) - 13.32\left(a/W\right)^2 + 14.72\left(a/W\right)^3 - 5.6\left(a/W\right)^4 \tag{34}$$

in which B_n is the net thickness of CT specimen. The comparisons of SIFs under different conditions are presented in Table 3. The results extracted from ABAQUS in this paper shown in Table 3 agree quite well with the solutions presented by Ref. [48] (i.e. solutions computed with Eqs. (32)-(34)), and the maximum relative error is less than 1% for all the calculated solutions. This can be an evidence to validate and assure the FE mesh quality of the numerical computations in this paper.

With the validation of FE meshes, the C^*-integral can be obtained with the contour integral method through extraction from ABAQUS directly. Note that C^*-integral calculated by ABAQUS with contour integral is a robust method. To assure the solution accuracy, ten integral contours ahead of creep crack are adopted in the calculations and the solution of the first contour is deleted. With the average of the contour integrals, the $C(t)$-integral for these four CT specimens are presented in Fig. 8. It can be seen that, the $C(t)$-integral is firstly path dependent under transient creep during the calculations. If the creep time exceeds the path independent time shown in Table 2, the $C(t)$-integral is considered to be the C^*-integral and will be path independent with a maximum relative error of 5%.

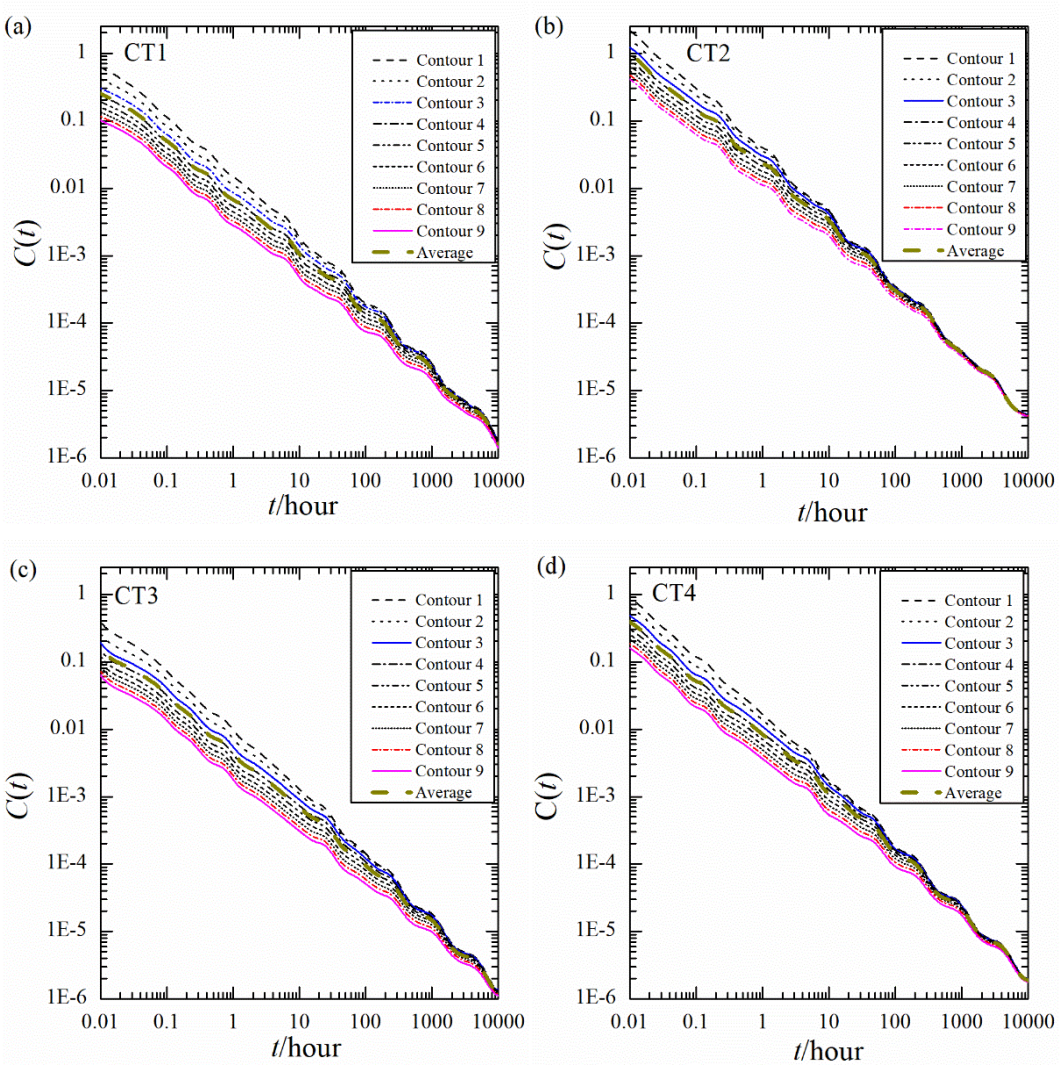

Fig. 8 Solutions of $C(t)$-integral for different CT specimens (a) CT1, (b) CT2, (c) CT3 and (d) CT4

6.2 Determination of constraint level

With Eqs. (16)-(19), A_2^*-parameter can be obtained at θ=0°. The characteristic length L is set to be 1 mm and the C^*-integrals have been given in Table 2 during the computation of A_2^*-parameter. The calculation of A_2^*-parameter can be as follows. For a fixed characteristic length and distance from crack tip, the open stress of σ_{22} can be determined by FE solutions as given in Section 6.1. The equation is written as

$$\sigma_{22} = c_1 + c_2 \cdot A_2^* + c_3 \cdot \left(A_2^*\right)^2 \tag{35}$$

where c_1, c_2 and c_3 are presented as:

$$c_1 = A_1^* \Lambda^{s_1} \tilde{\sigma}_{22}^{(1)}(\theta) \tag{36}$$

$$c_2 = A_1^* \Lambda^{s_2} \tilde{\sigma}_{22}^{(2)}(\theta) \tag{37}$$

$$c_3 = A_1^* \Lambda^{s_3} \tilde{\sigma}_{22}^{(3)}(\theta) \tag{38}$$

By solving Eqs. (35), A_2^*-parameter can be determined for a specific specimen. If one sets L=1 mm and r=1 mm, Eqs. (36)- (38) can be simplified as $A_1^* \tilde{\sigma}_{22}^{(1)}(\theta)$, $A_1^* \tilde{\sigma}_{22}^{(2)}(\theta)$ and $A_1^* \tilde{\sigma}_{22}^{(3)}(\theta)$, respectively. The constraint values of different CT specimens for A_2^*-parameter and $\bar{\Lambda}$-parameter are presented in Fig. 9. Generally, the constraint levels for the four specimens are ordered as CT2>CT4>CT1>CT3. The rank order for $\bar{\Lambda}$ is CT3>CT1>CT4>CT2. It is very interesting as the order of the constraint level is reversed between A_2^*-parameter and $\bar{\Lambda}$-parameter. However, it also should be noted that the values of them approaches very close to each other. The maximum difference between CT2 and CT3 for A_2^*-parameter is approaching to 6%. The maximum difference for $\bar{\Lambda}$-parameter of CT3 and CT2 approaches to be 10%.

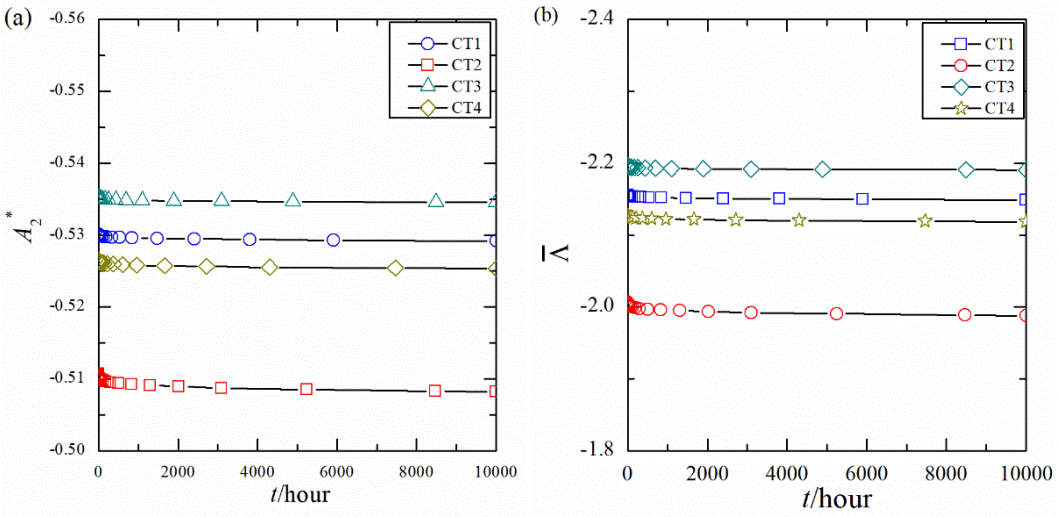

Fig. 9 Constraint levels of different CT specimens for (a) A_2^*-parameter and (b) $\bar{\Lambda}$-parameter

With Eqs. (21) and (24), the stress triaxiality h under different conditions are identical to -1.988, -1.996, -2.118 and -2.121 for CT1, CT2, CT3 and CT4 under

extensive creep, respectively. It should be noted that this solutions calculated by ABAQUS, which approaches to -2 very closely, i.e. Rice and Tracey's solution [49]. With Eq. (25), the solutions for $d\varepsilon_f^*/dh\cdot 1/\varepsilon_f^*(\theta,n)$ of the four CT specimens are 1.837, 1.837, 1.836 and 1.836, respectively. With the solution given above, the modification factors g' of Eq. (24) are obtained as 2.34, 2.18, 2.5 and 2.32 for CT1, CT2, CT3 and CT4, respectively.

6.3 Constraint modified TDFAD based on $C(t)$-$A_2(t)$ theory

For CT specimen under plane strain condition, the limit load can be given as [6]

$$P_L = B_n W \sigma_y \frac{2}{\sqrt{3}}\left[-\left(1+1.702\frac{a}{W}\right)+\sqrt{2.702\left(1+1.702\left(\frac{a}{W}\right)^2\right)}\right] \tag{39}$$

where a is the crack length and W is the plate width.

With the ligament ahead of crack tip for CT specimen, the nominal stress along the crack tip can be obtained as

$$\sigma_{\text{nominal}} = \frac{P}{B_n W} \tag{40}$$

With Eqs. (30) and (32), the $\bar{K}_r$ in TDFAD curve for CT specimen can be given as

$$\bar{K}_r = \frac{K_{\text{I}}}{K_{\text{mat}}^{\text{c}}} = \frac{Yf(a/W)}{K_{\text{mat}}^{\text{c}}}(g')^{-1/(2q)} \tag{41}$$

where g' is presented in the Eq. (24). Similar to Eqs. (31), (39) and (40), the $\bar{L}_r$ can be obtained as

$$\bar{L}_r = \frac{1}{\frac{2}{\sqrt{3}}\left[-\left(1+1.702\frac{a}{W}\right)+\sqrt{2.702\left(1+1.702\left(\frac{a}{W}\right)^2\right)}\right]}\frac{\sigma_{\text{nominal}}}{\bar{\sigma}_{0.2}} \tag{42}$$

With Eqs. (39)-(42) and modification factor g', the TDFAD curves for the four specimens considering constraint value of A_2^*-parameter are plotted in Fig. 10. It can be found that the assessment boundaries of TDFAD curves change significantly

although 316H steel is originally insensitive to TDFAD curves under creeping condition if the constraint effect is not taken into account according to [15], which implies that TDFAD curves nearly do not change with the increase of creep time. It indicates that TDFAD curves are sensitive to the constraint effect. It means that constraint effect is actually important during the characterization of TDFAD curves. As for $\bar{L}_r^{\max}$, the values are considered to obey the rule of R6 option 1 for the consideration of assessment conservative. Comparing with the R6 option, the potential failure zone of TDFAD curves considering constraint effect reduce significantly which means that the assessment curve of R6 is a conservative solution for integrity assessment.

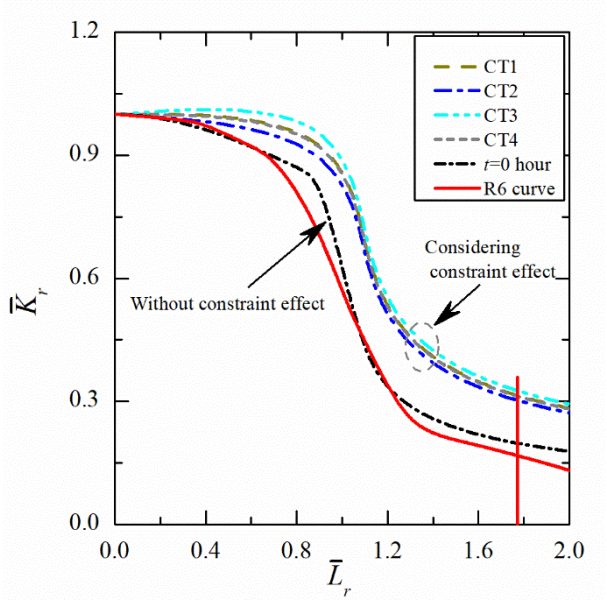

Fig. 10 Modified TDFAD curves for CT specimens considering constraint effect based on A_2^*-parameter

Based on the modification of the creep toughness and the characterization of constraint effect for mode I creep crack, the modified TDFAD based on $C(t)$-$A_2(t)$ theory is presented for CT specimens with 316H stainless steel as shown in Fig. 10. Note that 316H stainless steel is TDFAD insensitive material which does not change remarkably if the constraint effect is not taken into account even under creeping condition, and this point has been validated by Davies [15]. From Fig. 10, it can be found that the TDFAD curves vary significantly if the constraint effect is taken into account. It implies that TDFAD curve can be influenced by the constraint effect

remarkably for creep crack. Hence, constraint effect should be considered carefully during failure assessment of creep crack.

It should be pointed out that the modification of TDFAD is based on the modification of creep toughness as well as higher order term asymptotic solutions for creep crack, i.e. $C(t)$-$A_2(t)$ theory, which is rather different from the modification of Q-term. Thus, it provides a novel insight on the application of constraint effect to TDFAD curves. It has to emphasize that the modification is only for mode I creep crack. Recently, higher order asymptotic solutions for mixed I/II case have been studied by Dai et al. [1, 17]. It is very hopeful to see that the constraint modification can be extended to mixed I/II creep crack assessment in further investigations.

7 Concluding remarks

Based on the theoretical analysis and numerical computations, the influences of constraint effect on the assessment boundary of TDFAD curves are discussed and presented in this paper based on $C(t)-A_2(t)$ theory. The conclusions are drawn as below:

1) The constraint parameters for creep crack with $C(t)-Q$ theory and $C(t)-A_2(t)$ theory are compared. The relation of Q-parameter and $A_2(t)$-parameter is also derived and discussed.
2) Based on NSW model, a creep toughness modification method has been presented by incorporating $A_2(t)$-parameter. It can be found that the creep toughness for higher constraint value is lower than that without modification, and the creep toughness with lower constraint value is higher than that without modification.
3) A modified TDFAD technique is proposed based on $C(t)-A_2(t)$ theory by modifying creep toughness. The TDFAD curve has been validated by computing constraint level of CT specimen with 316H stainless steel considering various crack depths and loading levels. Results and discussions have shown that the influence

of constraint effect on TDFAD curves cannot be ignored as the evaluation border of TDFAD curves can be influenced by the constraint effect remarkably even for TDFAD insensitive material, e.g. 316H stainless steel.

This paper promotes an investigation on the influences of constraint effect on TDFAD curves based on $C(t)-A_2(t)$ theory, which indicates the important role of constraint effect on safety assessment for crack contained structure at elevated temperature. The research given in this paper can also provide an alternative method to incorporate higher order term asymptotic solutions into structural integrity assessment under high temperature.

Acknowledgement

The authors acknowledge the supports from the National Natural Science Foundation of China (Grant Nos. 11902009, 11672009, 11672147), the China Postdoctoral Science Foundation (No. 2019M650403) and the Beijing Key Laboratory of Advanced Manufacturing Technology.

Appendix A

Based on Eqs. (15) and (16), the stress triaxiality *h* can be presented as below with approximation that higher order term is much smaller than that of the first order term [26].

$$\frac{\sigma_m}{\sigma_e}=\frac{\tilde{\sigma}_m}{\tilde{\sigma}_e}+\frac{\tilde{F}_A}{\tilde{\sigma}_e}\left(\frac{C^*}{\sigma_0\dot{\varepsilon}_0 I_n}\right)^{-1/(n+1)} r^{1/(n+1)} \tag{A1}$$

where $\tilde{F}_A$ is a term including higher order terms and can be presented as below:

$$\tilde{F}_A=\frac{A_1^*\left[A_2^* r^{s_2}\tilde{\sigma}_{22}^{(2)}(\theta)+\left(A_2^*\right)^2 r^{s_3}\tilde{\sigma}_{22}^{(3)}(\theta)\right]}{\sigma_0} \tag{A2}$$

Note that the higher order term asymptotic solutions are considered to be smaller than that of the first order term and the equivalent stress is independent on the A_2^*-term. Hence, there exists the following formula with simplification [26].

$$\varepsilon_f = \tilde{\varepsilon}_f + \frac{\mathrm{d}\tilde{\varepsilon}_f}{\mathrm{d}h}\frac{\tilde{F}_A}{\tilde{\sigma}_e}\left(\frac{C^*}{\sigma_0\dot{\varepsilon}_0 I_n}\right)^{-1/(n+1)} r^{1/(n+1)} \tag{A3}$$

With Eqs. (A3), (20) and (21), the creep crack growth rate can be given as below:

$$\dot{a} = \dot{\varepsilon}_0\left(\frac{C^*}{\sigma_0\dot{\varepsilon}_0 I_n}\right)^{n/(n+1)}\frac{\tilde{\varepsilon}_e}{\tilde{\varepsilon}_f}H \tag{A4}$$

in which $\tilde{\varepsilon}_e$ and H are given as following

$$\tilde{\varepsilon}_e = \left(\tilde{\sigma}_e\right)^n \tag{A5}$$

$$H = \int_0^{r_c} r^{-n/(n+1)}\left[1 - \frac{\tilde{\varepsilon}_{f,h}}{\tilde{\varepsilon}_f}\frac{\tilde{F}_A}{\tilde{\sigma}_e}\left(\frac{C^*}{\sigma_0\dot{\varepsilon}_0 I_n}\right)^{-1/(n+1)} r^{1/(n+1)}\right]\mathrm{d}r \tag{A6}$$

With Eqs. (A4)-(A6) and through integration, Eqs. (23) and (24) can be obtained.

Appendix B

According to Eqs. (22) and (26), a creep crack growth rate with small amount increment can be given as [46]:

$$\dot{a}_0 = b\left(C^*\right)^q \tag{B1}$$

in which coefficient b and q are constants depending on creep crack growth rate. Thereafter, the creep crack extent Δa is kept as small increment without growth if the following form is satisfied based on Eq. (B1).

$$C^* < \left(\Delta a / bg't\right)^{1/q} \tag{B2}$$

Considering the reference stress method to obtain C^*-integral, the following formula can be obtained.

$$C^* = \frac{K^2}{Et}\frac{E\varepsilon_{\mathrm{ref}}}{\sigma_{\mathrm{ref}}} \tag{B3}$$

Considering Eq. (B2) and (B3), the following relation can be obtained.

$$\frac{K}{\left(E\left(\Delta a/bg'\right)^{1/q}t^{(1-1/q)}\right)^{1/2}}<\left(\frac{E\varepsilon_{\mathrm{ref}}}{\sigma_{\mathrm{ref}}}\right)^{-1/2} \tag{B4}$$

Combing Eqs. (B2)-(B4), the modified creep toughness in Eq. (27) is obtained as below [26]

$$K_{\mathrm{mat}}^{\bar{\Lambda}}=\left[E\left(\Delta a/bg'\right)^{1/q}t^{(1-1/q)}\right]^{1/2} \tag{B5}$$

If $g'=1$, the modified creep toughness will be degenerated to be creep toughness which is presented as below:

$$K_{\mathrm{mat}}^{\mathrm{c}}=\left[E\left(\Delta a/b\right)^{1/q}t^{(1-1/q)}\right]^{1/2} \tag{B6}$$

It should be pointed out that the derivations in Appendix B is similar to the derivation given by Ref. [26].

References

[1] YW Dai, YH Liu, F Qin, GA Qian, YJ Chao. *C* (*t*) dominance of the mixed I/II creep crack: Part I. Transient creep. Theoretical and Applied Fracture Mechanics, 103 (2019) 102314.

[2] L Zhao, L Xu, Y Han, H Jing. Quantifying the constraint effect induced by specimen geometry on creep crack growth behavior in P92 steel. International Journal of Mechanical Sciences, 94 (2015). 63-74.

[3] R6, Assessment of the integrity of structures containing defects, Revision 4 (2010).

[4] R. Ainsworth, D. Hooton, R6 and R5 procedures: The way forward, International Journal of Pressure Vessels and Piping, 85 (2008) 175-182.

[5] S. Webster, A. Bannister, Structural integrity assessment procedure for Europe–of the SINTAP programme overview, Engineering Fracture Mechanics, 67 (2000) 481-514.

[6] R. Ainsworth, A. Bannister, U. Zerbst, An overview of the European flaw assessment procedure SINTAP and its validation, International Journal of Pressure Vessels and Piping, 77 (2000) 869-876.

[7] F. Gutiérrez-Solana, S. Cicero, FITNET FFS procedure: a unified European procedure for structural integrity assessment, Engineering Failure Analysis, 16 (2009) 559-577.

[8] QD Xiao, YH Liu, YW Dai. Developments of strain-based failure assessment diagram applications: measuring reference strain by displacement and a modified assessment method. International Journal of Mechanical Sciences 140 (2018): 27-36.

[9] P Jia, HY Jing, LY Xu, YD Han, A modified reference strain method for engineering critical assessment of reeled pipelines. International Journal of Mechanical Sciences, 105 (2016): 23-31.

[10] J. Landes, J. Begley, A fracture mechanics approach to creep crack growth, ASTM STP, 590 (1976) 128-148.

[11] R.A. Ainsworth, The use of a failure assessment diagram for initiation and propagation of defects at high temperatures, Fatigue & Fracture of Engineering Materials & Structures, 16 (1993) 1091-1108.
[12] R.A. Ainsworth, D.G. Hooton, D. Green, Failure assessment diagrams for high temperature defect assessment, Engineering Fracture Mechanics, 62 (1999) 95-109.
[13] F.Z. Xuan, S.T. Tu, Z. Wang, Time-dependent fracture and defect assessment of welded structures at high temperature, Journal of Pressure Vessel Technology, 128 (2006) 556-565.
[14] C.M. Davies, N.P. O'Dowd, D.W. Dean, K.M. Nikbin, R.A. Ainsworth, Failure assessment diagram analysis of creep crack initiation in 316H stainless steel, International Journal of Pressure Vessels and Piping, 80 (2003) 541-551.
[15] C.M. Davies, Predicting creep crack initiation in austenitic and ferritic steels using the creep toughness parameter and time-dependent failure assessment diagram, Fatigue & Fracture of Engineering Materials & Structures, 32 (2009) 820-836.
[16] DW Dean, RA Ainsworth, SE Booth, Development and use of the R5 procedures for the assessment of defects in high temperature plant, International Journal of Pressure Vessels and Piping, 78 (2001) 963-976.
[17] YW Dai, YH Liu, F Qin, Y.J Chao. A unified method to solve higher order asymptotic crack-tip fields of mode I, mode II and mixed mode I/II crack in power-law creeping solids. Engineering Fracture Mechanics, 218 (2019) 106610.
[18] YW Dai, DH Liu, YH Liu, Mismatch constraint effect of creep crack with modified boundary layer model. Journal of Applied Mechanics 83.3 (2016): 031008.
[19] YW Dai, YH Liu, Yuh J. Chao. Higher order asymptotic analysis of crack tip fields under mode II creeping conditions. International Journal of Solids and Structures 125 (2017): 89-107.
[20] GA Qian, WS Lei. A statistical model of fatigue failure incorporating effects of specimen size and load amplitude on fatigue life. Philosophical Magazine (2019) 1-37.
[21] GA Qian, WS Lei, L. Peng, Yu Z, M Niffenegger, Statistical assessment of notch toughness against cleavage fracture of ferritic steels. Fatigue & Fracture of Engineering Materials & Structures, 41(5) (2018) 1120-1131.
[22] I.J. MacLennan, J.W. Hancock, Constraint-based failure assessment diagrams, Proceedings of the Royal Society of London A: Mathematical, Physical and Engineering Sciences, 451 (1995) 757-777.
[23] Cicero S, Gutiérrez-Solana F, Álvarez JA. Structural integrity assessment of components subjected to low constraint conditions. Engineering Fracture Mechanics, 75.10 (2008) 3038-3059.
[24] X.K. Zhu, S.K. Jang, J–R curves corrected by load-independent constraint parameter in ductile crack growth, Engineering Fracture Mechanics, 68 (2001) 285-301.
[25] C.F. Shih, N. O'Dowd, M. Kirk, A framework for quantifying crack tip constraint, Constraint effects in fracture, (1991) 2-20.
[26] P. Budden, R. Ainsworth, The effect of constraint on creep fracture assessments, International Journal of Fracture, 87 (1997) 139-149.
[27] F.Z. Xuan, S.T. Tu, Z.D. Wang, J.M. Gong, On the creep fracture toughness of 2¼Cr1Mo steel, Key Engineering Materials, (2005) 1464-1469.
[28] C.M. Davies, D.W. Dean, K.M. Nikbin, N.P. O'Dowd, Interpretation of creep crack initiation and growth data for weldments, Engineering Fracture Mechanics, 74 (2007) 882-897.

[29] Y.J. Kim, P.J. Budden, Plastic η factor solutions of homogeneous and bi-material SE(T) specimens for toughness and creep crack growth testing, Fatigue & Fracture of Engineering Materials & Structures, 24 (2001) 751-760.

[30] Y. Chao, X. Zhu, L. Zhang, Higher-order asymptotic crack-tip fields in a power-law creeping material, International Journal of Solids and Structures, 38 (2001) 3853-3875.

[31] B. Nguyen, P. Onck, E. Van Der Giessen, On higher-order crack-tip fields in creeping solids, Journal of Applied Mechanics, 67 (2000) 372-382.

[32] Mohyud-Din S.T., Noor M.A., Noor K. I. Some relatively new techniques for nonlinear problems. Mathematical Problems in Engineering, 2009.

[33] Mohyud-Din S.T., Bibi S., Ahmed N., Khan U. Some exact solutions of the nonlinear space–time fractional differential equations. Waves in Random and Complex Media, 29(4) (2019) 645-664.

[34] Bibi S, Mohyud-Din S.T., Khan U, Ahmed N. Khater method for nonlinear Sharma Tasso-Olever (STO) equation of fractional order. Results in Physics, 7 (2017) 4440-4450.

[35] YW Dai, YH Liu, Y.J Chao. Theoretical analysis and engineering implications for the high order term solutions of the mode II type creep crack. Proceedings of ASME Pressure Vessels and Piping Conference. (2017) V06AT06A047.

[36] G.Z. Wang, X.L. Liu, F.Z. Xuan, S.T. Tu, Effect of constraint induced by crack depth on creep crack-tip stress field in CT specimens, International Journal of Solids and Structures, 47 (2010) 51-57.

[37] H.S. Ma, G.Z. Wang, F.Z. Xuan, S.T. Tu, Unified characterization of in-plane and out-of-plane creep constraint based on crack-tip equivalent creep strain, Engineering Fracture Mechanics, 142 (2015) 1-20.

[38] J.P. Tan, G.Z. Wang, S.T. Tu, F.Z. Xuan, Load-independent creep constraint parameter and its application, Engineering Fracture Mechanics, 116 (2014) 41-57.

[39] Guo WL, Chen Z, She C. Universal characterization of three-dimensional creeping crack-front stress fields. International Journal of Solids and Structures, 152 (2018) 104–117

[40] ASTM, E1457-13: Standard Test Method for Measurement of Creep Crack Growth Times and Rates in Metals, (2013).

[41] F.H. Norton, The creep of steel at high temperatures, McGraw-Hill Book Company, Incorporated, 1929.

[42] Y. Chao, L. Zhang, Tables of plane strain crack tip fields: HRR and higher order terms, Department of Mechanical Engineering, University of South Carolina, Technical Report No. ME-Report, (1997) 97-91.

[43] P Ding, Xin Wang, Solutions of the second elastic–plastic fracture mechanics parameter in test specimens. Engineering Fracture Mechanics 77.17 (2010): 3462-3480.

[44] K. Nikbin, D. Smith, G. Webster, Prediction of creep crack growth from uniaxial creep data, in: Proceedings of the Royal Society of London A: Mathematical, Physical and Engineering Sciences, 1984, 183-197.

[45] A. Cocks, M. Ashby, Intergranular fracture during power-law creep under multiaxial stresses, Metal Science, 14 (1980) 395-402.

[46] M. Yatomi, N.P. O'Dowd, K.M. Nikbin, G.A. Webster, Theoretical and numerical modelling of creep crack growth in a carbon–manganese steel, Engineering Fracture Mechanics, 73 (2006) 1158-1175.

[47] M. Yatomi, M. Tabuchi, Issues relating to numerical modelling of creep crack growth, Engineering Fracture Mechanics, 77 (2010) 3043-3052.
[48] H. Tada, P. Paris, G. Irwin, The analysis of cracks handbook, New York: ASME Press, 2000.
[49] J.R. Rice, D.M. Tracey, On the ductile enlargement of voids in triaxial stress fields, Journal of the Mechanics and Physics of Solids, 17 (1969) 201-217.